analytical chemistry

pubs.acs.org/ac Article

Degradation of Reporter Molecules Imposes a Fundamental Limit of Detection on CRISPR Diagnostics

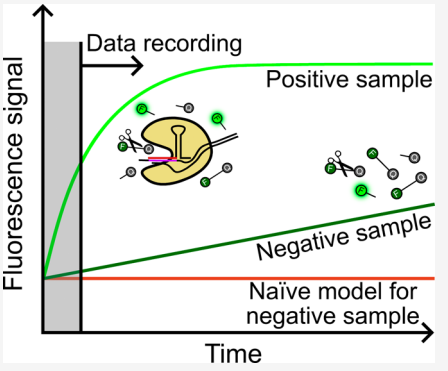
Alexandre S. Avaro, Andrew D. Griffiths, and Juan G. Santiago*

Cite This: https://doi.org/10.1021/acs.analchem.5c01060 Read Online

ACCESS | Metrics & More | Article Recommendations | Supporting Information

Downloaded via SHANGHAI NORMAL UNIV on June 20, 2025 at 00:39:20 (UTC).
See https://pubs.acs.org/sharingguidelines for options on how to legitimately share published articles.

ABSTRACT: The sensitivity of CRISPR-Cas systems used for molecular diagnostics remains a major bottleneck in the adoption of this technology. The vast majority of CRISPR-based assays use dually labeled, single-stranded reporters and fluorescence signal readouts to infer enzymatic activity and the presence (or absence) of target nucleic acid. The limit of detection of such assays is set by the kinetics of the Cas enzymes and a slow yet measurable increase in the fluorescence signal. We demonstrate here that the background signal and limits of detection of most assays are very likely limited by the degradation of reporter molecules. This degradation is dynamic and is not associated with enzymatic activity. We present theory and experiments to design and calibrate CRISPR assays. We introduce a new kinetic framework to account for the degradation of reporter molecules and derive a fundamental limit of detection for CRISPR-based assays. Our data show that Michaelis−Menten kinetics alone are insufficient to describe reporter (substrate) cleavage rates. The framework and techniques presented here should help reduce the frequency and magnitude of errors currently routinely made in quantifying CRISPR kinetics and interpreting CRISPR diagnostic fluorescence signals.



INTRODUCTION

Clustered regularly interspaced short palindromic repeats-associated enzymes (CRISPR-Cas) have raised significant attention in the field of molecular diagnostics in the past few years.[1−4] CRISPR-Cas systems typically consist of a Cas endonuclease (e.g., Cas12[5,6] or Cas13[7]) conjugated to a synthetic guide RNA (gRNA), which includes a sequence complementary to the target nucleic acid. The enzyme first recognizes and cleaves the target in a specific *cis*-cleavage step, which activates the enzyme. The activated enzyme subsequently exhibits a nonspecific collateral *trans*-cleavage of single-stranded nucleic acids (e.g., DNA for Cas12 and RNA for Cas13).[1,3,8] A great variety of strategies have been developed to leverage this mechanism for diagnostic purposes. The majority of these assays use synthetic single-stranded nucleic acid reporters labeled with a fluorophore on one end and a quencher on the other.[6,9,10] In such assays, a rise in fluorescence signal is used to detect enzymatic *trans*-activity and this signal informs on the presence of the target, the target's initial concentration, and/or the reaction kinetics of the enzyme. CRISPR-based detection methods are often presented as an alternative to exponential molecular amplification methods such as quantitative polymerase chain reaction (qPCR) and loop-mediated isothermal amplification (LAMP).[11−13] The latter methods are robust but can be prone to false positives and often require bulky and expensive equipment for target quantitation. By comparison, CRISPR-based methods are highly specific, easily reconfigurable, and do not require thermal cycling, and this makes them an increasingly popular addition to the molecular diagnostics toolbox.[4,10,14]

An important disadvantage of CRISPR-based assays over molecular amplification techniques is their limited sensitivity,[4,15] which is limited by both their kinetic rates and observed nonspecific background activity. Early reports[6,16] claimed that CRISPR catalytic rates exceeded 1000 turnovers per second, but these and other similar reports are now known to be gross errors.[17−19] Catalytic rates are typically on the order of 1 turnover per second.[17] Furthermore, CRISPR-Cas systems that leverage the cleavage of fluorophore-quencher reporters exhibit finite background activity,[17,19−21] where a measured fluorescence signal increases with time even in the absence of target molecules. These limitations constitute a major obstacle to the detection of trace concentrations of nucleic acids.[19] Despite the fundamental importance of the background activity on the limit of detection of CRISPR assays, to our knowledge, there has been no kinetic description or model that accounts for this phenomenon.

In this work, we report on and present experimental evidence of the essential role played by the nonenzymatic

Received: February 20, 2025
Revised: June 2, 2025
Accepted: June 5, 2025

© XXXX American Chemical Society

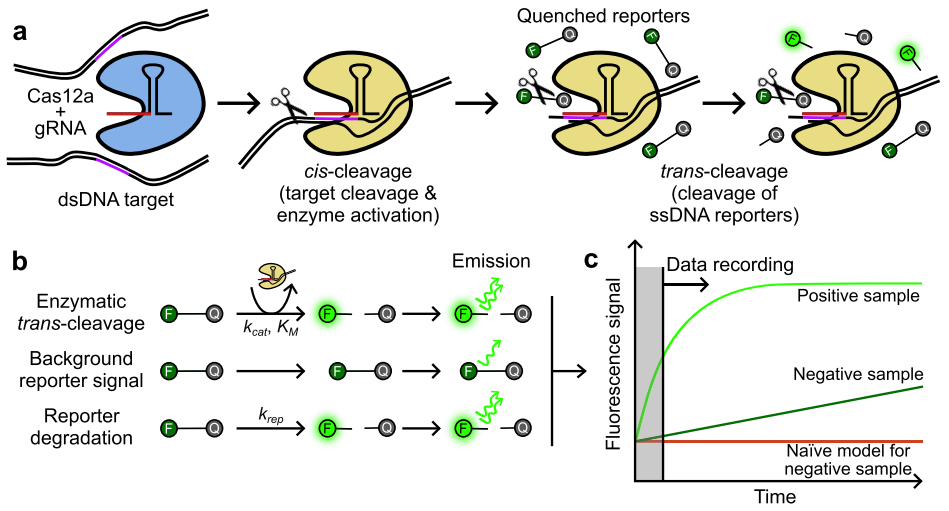


Figure 1. CRISPR diagnostic fluorescent signals. (a) Schematic for DNA detection using CRISPR-Cas12. The Cas12/gRNA complex (ribonucleoprotein, RNP) first recognizes a specific ∼20-nucleotide DNA sequence complementary to the gRNA. This activates the enzyme (shown in yellow color), triggering nonspecific cleavage of ssDNA fluorophore-quencher reporters. (b) Schematic of three sources of fluorescent signal. In addition to background signal (e.g., from plastic thermocycler tubes, not shown), photons are emitted by reporters cleaved by the Cas12 enzyme upon activation; uncleaved reporters that are imperfectly quenched; or reporters that are degraded nonenzymatically. (c) Schematic of fluorescence signals versus time from a positive sample (with target), a negative sample (no target), and the prediction by a (commonly used) naïve model for a negative sample.

degradation of fluorescent reporters. We show that this degradation happens independently of CRISPR activity. Yet, because it becomes the dominant reaction mechanism at low target concentrations, it has immense consequences on CRISPR assay sensitivity. Furthermore, the kinetics of this reporter degradation imply that the traditional Michaelis−Menten kinetic system does not capture empirical observations. We use our model to derive an analytical expression for a fundamental limit of detection imposed by reporter degradation on CRISPR assays. We provide a novel approach to calibrate CRISPR assay signals that incorporates a modified kinetic framework (different from Michaelis−Menten). We also present a controlled experimental study demonstrating this degradation, experimental validation of our model, and how this degradation directly limits the sensitivity of a Cas12 assay.

METHODS

Reagents. LbCas12a (a Cas12 ortholog from*Lachnospiraceae bacterium ND2006*) at a concentration of 100 μM and NEBuffer r2.1 were purchased from New England Biolabs (MA, USA). NEBuffer r2.1 is composed of 50 mM NaCl, 10 mM Tris-HCl, 10 mM $MgCl_2$, and 100 μg/mL recombinant albumin (pH 7.9 at 25 °C). Reporter molecules were purchased from Eurofins Genomics (France) and resuspended at 100 μM. All other oligonucleotides reported in Table S1 (Section S7) were obtained from Integrated DNA Technologies (IDT) and resuspended at 100 μM. All fluorescence measurements were performed using a CFX384 Touch Real-Time PCR Detection System (Bio-Rad Laboratories). In all experiments, fluorescence measurements were taken at 37 °C and every 30 s.

***Trans*-Cleavage Kinetics Experiments.** We first prepared a solution of 1 μM ribonucleoprotein (RNP) by incubating 1 μM synthetic gRNA and Cas12a at 37 °C for 30 min. RNPs were first diluted to 80 nM in NEBuffer r2.1 before activation with 20 nM synthetic dsDNA target at 37 °C for 30 min. The kinetics of *cis*-cleavage have been extensively discussed elsewhere,[22−26] and we here consider the reaction complete after incubation. We then performed *trans*-cleavage kinetics assays using 1 nM activated RNP and varying synthetic reporter concentrations (ranging from 14 to 900 nM in 2-fold dilutions). The reactions were buffered in 1X NEBuffer r2.1. All mixing steps prior to data acquisition were performed on ice. Three replicates were obtained for each reporter concentration. Fluorescence values were converted to concentrations using the models described in the main manuscript and the calibration curves reported in Section S8. The initial reaction velocities were computed by using a linear fit to the first ∼3 min of the reaction progress curves. Kinetic rates k_{cat} and K_M were computed using a nonlinear Michaelis−Menten fit using GraphPad Prism 10 (GraphPad Software, CA, USA). Note that the Michaelis−Menten model is sufficient here, as target concentrations are sufficiently high.

Reporter Degradation Experiments. We conducted experiments similar to those performed in the *trans*-cleavage kinetic experiments, omitting one or several critical components of the CRISPR reaction. For the no-target experiment (Figure 3b), we prepared a solution of 80 nM RNP following the same protocol as described above. We then diluted the RNPs to 5 nM (final concentration) and mixed them with solutions containing varying synthetic reporter concentrations (ranging from 14 to 900 nM in 2-fold dilutions). For the no-gRNA experiment (Figure 3c), we mixed 50 nM Cas12a with 1 nM dsDNA target and the same varying concentrations of ssDNA reporters. For the no-Cas experiment (Figure 3d), we mixed 10 nM gRNA with 1 nM target and varying concentrations of reporters. Finally, for the reporter-only experiment (Figure 3e), we diluted the ssDNA reporter stock to varying concentrations ranging from 14 to 900 nM in 2-fold serial dilutions. Three replicates were taken for each reporter concentration for all cases.

In all cases, we then proceeded with fluorescence measurements. Reactions were performed in 1X NEBuffer r2.1. Initial reaction velocities were computed using a linear fit to the first

https://doi.org/10.1021/acs.analchem.5c01060
Anal. Chem. XXXX, XXX, XXX−XXX

~15 min of the reaction progress curves. The value of k_{rep} was computed using a linear fit using GraphPad Prism 10.

Limit of Detection Experiments. We first prepared a solution of 1 μM RNP by incubating 1 μM synthetic gRNA and Cas12a at 37 °C for 30 min. RNPs were first diluted to 80 nM in NEBuffer r2.1 before incubation with 110 nM reporters and concentrations of synthetic target dsDNA ranging from 1 fM to 10 nM in 10-fold dilutions. Reactions were performed in 1X NEBuffer r2.1. Fluorescence values were converted to concentrations using the calibration process described in Section S8. The initial reaction velocities were computed by using a linear fit to the first ~500 s of the reaction progress curves.

RESULTS AND DISCUSSION

Signal Kinetics in the Low Target Concentration Limit. Figure 1a summarizes a typical CRISPR-Cas12 diagnostic assay. The assay involves two sequential reactions.[6,8] The first is a relatively rapid[22−25] reaction called *cis*-cleavage during which the enzyme is activated by recognizing and cleaving a specific target DNA sequence complementary to the gRNA. The second is the rate-limiting step called *trans*-cleavage where the enzyme indiscriminately cleaves single-stranded nucleic acid reporter molecules. The vast majority of the published Cas12 assays use short, dually labeled ssDNA fluorophore-quencher reporters, whose quantum yield significantly increases when cleaved.[1,6,27] An increase in the fluorescence signal is used to detect enzyme activation, and the presence of target nucleic acid is deduced from this signal.

The most successful model to describe the *trans*-cleavage kinetics of the Cas enzyme is the Michaelis−Menten model.[18,28] In this framework, the rate of production of cleaved reporter is proportional to the activated enzyme concentration, and this can allow the quantification of the initial DNA target concentration. For such questions, we often want relations between the measured signals and the kinetic rates of the reaction. However, as reported by Santiago,[19] a large fraction of all CRISPR diagnostic studies[6,16,21,27,29,30] report absolutely no calibration method or calibration data. This deficit in reporting can make it impossible to verify and even reproduce studies. It can also lead to gross errors in kinetic rates.[31,32] We summarize in Section S1 a brief history of kinetic model formulations and calibration methods (including successive improvements) for CRISPR-based diagnostic methods. To our knowledge, the most comprehensive calibration has been reported by Blanluet et al.[33] Here, we derive a closed-form expression for the fluorescence signal in the limit of low initial target concentration, as predicted by the Michaelis−Menten framework.

Under the quasi-steady state and the reactant stationary assumptions,[34] we first adapt the calibration eq 10 from Avaro and Santiago[22] and include the extension proposed by Blanluet et al.[33] We present a detailed derivation of this approach in Section S1. This calibration

$$I^{corr}_{naïve}(t;\,[E]_0) = 10^{-\frac{[S]_0}{c_0}}\left(F'_{Ucl}K_M\mathcal{A}(t) + F'_{Cl}\left([S]_0 - K_M\mathcal{A}(t) - [E]_0\frac{\mathcal{A}(t)}{1+\mathcal{A}(t)}\right)\right) \quad (1)$$

where:

$$\mathcal{A}(t) = W\left(\frac{[S]_0}{K_M}\exp\left(\frac{[S]_0}{K_M} - \frac{k_{cat}}{K_M}[E]_0 t\right)\right) \quad (2)$$

Here, $I^{corr}_{naïve}(t,\,[E]_0)$ denotes the so-called "flatfield-corrected"[22,33] fluorescence intensity at time t as predicted by the Michaelis−Menten model. F'_{Cl}, F'_{Ucl}, and c_0 are calibration constants, k_{cat} and K_M are the kinetic rates of the enzyme, $[E]_0 = [E](t = 0)$ is the initial activated enzyme concentration, $[S]_0 = [S](t = 0)$ represents the total concentration of reporters in the reaction, and W is the Lambert-W function.[35] We note that the model represented by eq 1 accounts for the signal originating from uncleaved reporters, the so-called "inner-filter effect," and the well-to-well (i.e., position-to-position) variation in fluorescence detector response.[33] In the limit where the target concentration $[E]_0$ is low, this closed-form solution is well approximated at the first order by:

$$I^{corr}_{naïve}(t;\,[E]_0) \approx 10^{-\frac{[S]_0}{c_0}}[S]_0\left(F'_{Cl}\left(1 - \frac{[E]_0}{K_M + [S]_0}\right) - (F'_{Cl} - F'_{Ucl})\left(1 - \frac{k_{cat}[E]_0 t}{K_M + [S]_0}\right)\right) \quad (3)$$

The derivation of eq 3 involves a Taylor series expansion of the Lambert-W function and we discuss these details in Section S2.

Next, we discuss the rates of increase of the signal of these systems. We often want a signal that is a weak function of the initial signal value and the initial background value. As such, we consider the first derivative with respect to time of eq 3:

$$\frac{dI^{corr}_{naïve}}{dt}([E]_0) \approx 10^{-\frac{[S]_0}{c_0}}(F'_{Cl} - F'_{Ucl})k_{cat}[E]_0\frac{[S]_0}{K_M + [S]_0} \quad (4)$$

As expected, this model of signal rate is proportional to the initial velocity predicted by the Michaelis−Menten model:

$$\frac{d[P]_{naïve}}{dt} = k_{cat}[E]_0\frac{[S]_0}{K_M + [S]_0} \quad (5)$$

We here refer to eqs 3−5 as the "naïve" model for CRISPR kinetics, which we seek to criticize and expand upon in this paper. This naïve model is consistent with the prevalent theory of CRISPR reactions, which assumes that the target concentration limits the maximum value of $[E]_0$; and, if $[E]_0 = 0$, the signal is not expected to increase in time.

As we shall discuss and demonstrate with quantitative experiments, the prediction and interpretation that signals will not increase for negative samples (i.e., lacking target molecules) is incorrect. There is in fact published experimental data showing that reaction velocities (as interpreted from

https://doi.org/10.1021/acs.analchem.5c01060
Anal. Chem. XXXX, XXX, XXX−XXX

fluorescence signals and calibration) plateau to a constant, nonzero value as target concentrations approach zero.[17,18,20,21,36] The mechanism behind this nonspecific signal rise has not been explained, but the evidence implies that there exists another source of fluorescent signal that is unaccounted for by the aforementioned models or calibrations and not predicted by the Michaelis−Menten framework.

Figure 1b summarizes the three different sources of the fluorescence signal of a CRISPR reaction. The first source consists of reporters cleaved by enzymatic *trans*-cleavage. The second source involves the imperfectly quenched, yet uncleaved reporters ($I_{\text{naïve}}(t;\ 0)$), which was introduced and accounted for in eq 1 above and which we detail in Section S8. The third source of signal is the effect that is the focus of this work: the degradation of reporters independent of the CRISPR enzyme. The latter two sources of signal are not directly related to the activated enzyme concentration and are therefore usually considered as background signal for any diagnostic assay or enzyme kinetics measurement. However, we know of no published work that accounts for the observed degradation rate of reporters. Figure 1c shows schematic progress curves (i.e., evolution of fluorescence signal vs time) that result from the summation of the three sources of signal listed in Figure 1b. Shown here are progress curves in the presence of the target (light green) and the absence of the target (negative, dark green). We also show the prediction by the naïve model (eq 1) for the negative case. As mentioned earlier, the naïve model predicts zero signal increase in the absence of target molecules.

Proposed Modifications to Michaelis−Menten Kinetics to Include First-Order Reporter Degradation. We now introduce an important factor in the interpretation of CRISPR kinetics, which we recently discovered and quantified as part of the current study. The discrepancy between the experimental observations and the naïve Michaelis−Menten predictions implies the existence of an underlying complexity in the kinetics description of any CRISPR system that involves the fluorescently labeled reporters. Namely, a critical source of background signal originates from reporters, which can degrade in the absence of the target and/or the CRISPR-Cas enzyme.

To account for this observation, we introduce here a so-called "augmented" (as opposed to "naïve") kinetics framework to describe enzymatic assays with first-order reporter molecule degradation. We select a first-order model to keep it as simple as possible while capturing essential experimental observations. We describe this reaction system using the following equations:

$$E + S \underset{k_b}{\overset{k_f}{\rightleftharpoons}} C \xrightarrow{k_{cat}} E + P \tag{6}$$

$$S \xrightarrow{k_{rep}} P \tag{7}$$

Here, eq 7 corresponds to the observed degradation of reporters that is not mediated by the Cas enzyme. The corresponding system of rate equations is then more fully described as:

$$\frac{d[S]}{dt} = -k_f[E][S] + k_b[C] - \boldsymbol{k_{rep}}[\boldsymbol{S}] \tag{8}$$

$$\frac{d[E]}{dt} = -k_f[E][S] + (k_{cat} + k_b)[C] \tag{9}$$

$$\frac{d[C]}{dt} = k_f[E][S] - (k_{cat} + k_b)[C] \tag{10}$$

$$\frac{d[P]}{dt} = k_{cat}[C] + \boldsymbol{k_{rep}}[\boldsymbol{S}] \tag{11}$$

With the following initial conditions:

$$[S](t = 0) = [S]_0 \tag{12}$$

$$[E](t = 0) = [E]_0 \tag{13}$$

$$[C](t = 0) = 0 \tag{14}$$

$$[P](t = 0) = 0 \tag{15}$$

Similar to the Michaelis−Menten system, we define $K_M = \frac{k_{cat} + k_b}{k_f}$. Closed-form solutions[37] for similar systems of rate equations have been derived, but they rely on transcendental functions that are specially defined for these systems and that are not available in most scientific computing packages. Under the reactant stationary assumption and the quasi-steady state assumption,[35] we can derive an analytical expression for the initial reaction velocity analogous to the naïve Michaelis−Menten case (eq 5):

$$\frac{d[P]}{dt}(t = 0) = k_{cat}[E]_0 \frac{[S]_0}{K_M + [S]_0} + k_{rep}[S]_0 \tag{16}$$

In the special case where $[E]_0 = 0$ (no target), eqs 8−11 collapse to:

$$\frac{d[S]_{BG}}{dt} = -\frac{d[P]_{BG}}{dt} = -k_{rep}[S]_{BG} \tag{17}$$

Eq 17 then yields an analytical solution for the fluorescence intensity in the no-target case:

$$I^{corr}_{meas,BG}(t) = \frac{I(t) - I_{BG}(t)}{I_{FF}(t) - I_{BG}(t)} = 10^{-\frac{[S]_0}{c_0}}[S]_0(F'_{Cl} - (F'_{Cl} - F'_{Ucl})e^{-k_{rep}t}) \tag{18}$$

In eq 18, I_{FF} and I_{BG} are, respectively, the flatfield and background signal arrays (associated with the array of reaction-tube-specific detectors). Unlike eq 1 in Blanluet et al.,[33] the quantities I_{BG} and I_{FF} are here time-dependent arrays and not averages in time. The time rate of change of the signal is then:

$$\frac{dI^{corr}_{meas,BG}}{dt}(t) = 10^{-\frac{[S]_0}{c_0}}(F'_{Cl} - F'_{Ucl})k_{rep}[S]_0 e^{-k_{rep}t} \tag{19}$$

where $I^{corr}_{meas,BG}$ is the flatfield-corrected fluorescence intensity in the no-target limit. This corresponds to the following characteristic time scale τ_d:

$$\tau_d = 1/k_{rep} \tag{20}$$

Here, the subscript "d" denotes "degradation." For characteristic observed rates, as we will show below, this characteristic time is much longer than typical experiments (e.g., $\tau_d > 8$ days for $k_{rep} = 1.4 \times 10^{-6}\ s^{-1}$). We indicate with τ_e the characteristic duration of the experiment (5 min $< \tau_e <$ 2 h for typical *trans*-cleavage experiments). Assuming $\tau_e \ll \tau_d$, then the rate of

https://doi.org/10.1021/acs.analchem.5c01060
Anal. Chem. XXXX, XXX, XXX−XXX

increase of the background signal, as derived in eq 19, is approximately constant throughout the measurement:

$$\frac{dI^{\mathrm{corr}}_{\mathrm{meas,BG}}}{dt} \approx 10^{-\frac{[S]_0}{c_0}}(F'_{\mathrm{Cl}} - F'_{\mathrm{Ucl}})k_{\mathrm{rep}}[S]_0 \tag{21}$$

We will, later in this paper, refer to this estimate of the initial rate of signal growth.

Before validating our model with experimental data, we present simple visualizations of the theory. Specifically, Figure 2a shows plots of the predicted initial (linear) portions of the progress curves. Shown are product concentration profiles ($[P](t)$) for seven concentrations of the target (i.e., $[E]_0$). We show two sets of predictions. First, the solid lines are predictions by the naïve Michaelis–Menten model. Second, the data symbols show results from our augmented model (eqs 8–15). Note that the data symbols are color-coded to the corresponding curves of the naïve model. Figure 2b shows a subset of five of these curves in the low product concentration region ($[P](t) < 1$ nM) for clarity of presentation. As derived in eq 5, the initial reaction velocity predicted by the naïve model is proportional to the target concentration and therefore approaches zero as $[E]_0$ approaches zero. However, unlike the naïve model, the augmented model curves converge toward a nonzero, linear increase in product concentration as the target concentration approaches zero (shown using cross data symbols). This corresponds to the zero-target limit derived in eqs 17–19, where the degradation of reporters dominates the production of cleaved reporters over the enzymatic *trans*-cleavage reaction. We indicate with shading in Figures 2a and b the region where detection is extremely difficult for the specified values of k_{rep} and $[S]_0$. In this low-target regime, accurate detection would require precise knowledge of the degradation of reporters and would require that this degradation be extremely repeatable from experiment to experiment. Note that the degradation of CRISPR reporters has analogies to that of qPCR TaqMan probes, which we discuss briefly in Section S7.

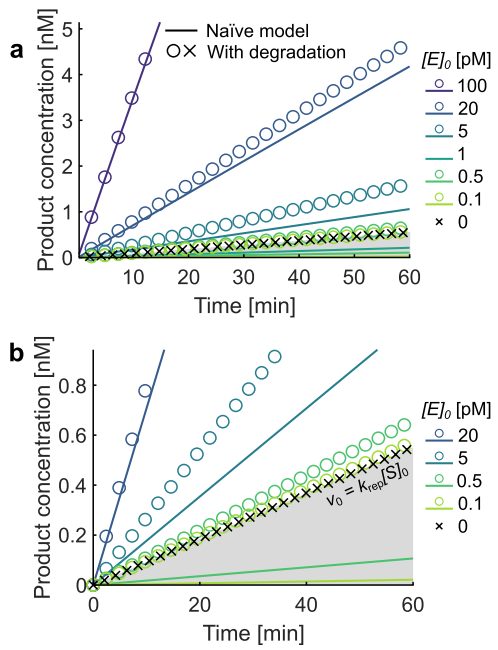


Figure 2. Comparison of naïve versus augmented models. (a) Example cleaved reporter concentrations versus time for a fixed initial reporter concentration ($[S]_0$ = 110 nM) and seven values of target concentration $[E]_0$. Shown are numerical solutions to the full Michaelis–Menten system (eqs 8–15), with (symbols) or without (naïve model, lines) reporter degradation. (b) Selected curves from (a), in the zone of low product concentrations. As target concentration ($[E]_0$) approaches zero, the curves converge to a minimum signal rise determined by reporter degradation (and not by *trans*-cleavage by CRISPR). The shaded region highlights the region that is practically inaccessible in the augmented kinetic framework. We used the following values for this example: $k_f = 10^{10}$ M^{-1}s^{-1}, k_{cat} = 2.0 s^{-1}, K_{M} = 3.6 μM, and $k_{\mathrm{rep}} = 1.4 \times 10^{-6}$ s^{-1}.

A Fundamental Limit of Detection for CRISPR Fluorescence-Based Assays. We here derive a simple algebraic expression describing a fundamental limit of detection for any enzymatic assay given first-order reporter degradation. As an important reference value, we define $[E]_{0,\mathrm{LoD}}$ as the theoretical initial target concentration for which *trans*-cleavage with no reporter degradation exactly matches an observed signal increase due solely to reporter degradation (*sans* target). $[E]_{0,\mathrm{LoD}}$ can therefore be interpreted as an apparent target concentration that would, in the framework of the naïve model, explain a signal that is actually due solely to reporter degradation. To this end, we set equal the right-hand sides (RHSs) of eqs 4 and 21, and derive the following:

$$[E]_{0,\mathrm{LoD}} = (K_{\mathrm{M}} + [S]_0)\frac{k_{\mathrm{rep}}}{k_{\mathrm{cat}}} \tag{22}$$

The latter also corresponds to the situation where each of the two terms in the RHS of eq 16 has an equal contribution to the cleaved reporter production. We will term this condition as a signal-to-background ratio of unity. $[E]_{0,\mathrm{LoD}}$ is an extremely useful estimate for the design of all CRISPR kinetics and CRISPR diagnostic assays that rely on reporter molecules. First, this concentration is directly proportional to the reporter degradation rate k_{rep}—highlighting the great importance of this reporter degradation effect. Second, this concentration is a linear function of the reporter concentration. Depending on the magnitude of K_{M}, increasing the reporter concentration $[S]_0$ can have a strongly deleterious effect on sensitivity.

Late-Readout Effect on the Reaction Velocity. In this section, we introduce a scaling argument to evaluate the reliability of experimentally measured reaction velocities as approximations of initial reaction velocities. The characteristic time scale of completion of the Michaelis–Menten reaction τ_{MM} is determined by the kinetic rates of the enzyme:[18,19]

$$\tau_{\mathrm{MM}} = \frac{K_{\mathrm{M}}}{k_{\mathrm{cat}}[E]_0} \tag{23}$$

However, the *trans*-cleavage reaction is initiated upon mixing reagents and there is a time delay before signal acquisition begins. This delay corresponds to the time necessary to mix reagents into a reaction vessel, load the vessel (tube or well-plate) into a detection instrument, heat the vessel to incubation temperature, and initiate data collection. We denote this time delay τ_{pre} (where the subscript denotes "preparation time" or "pre-data-collection"). In our experience, τ_{pre} is typically on the order of a few minutes ($\tau_{\mathrm{pre}} \approx 5$ min). For high values of $[E]_0$, the characteristic time of completion of the reaction τ_{MM} can be on the same order of magnitude than τ_{pre}. For instance, for $[E]_0$ = 10 nM and typical measured values for the kinetic rates for LbCas12a (k_{cat} = 2.0 s^{-1}, K_{M} = 3.6 μM), $\tau_{\mathrm{MM}} \approx 3$ min. In this case, the measured reaction

https://doi.org/10.1021/acs.analchem.5c01060
Anal. Chem. XXXX, XXX, XXX−XXX

velocity (after a delay τ_{pre}) substantially underpredicts the real initial reaction velocity (as depicted in Figure 1c). We will here term this underprediction of the reaction velocity the "late-readout effect." As an illustration, we provide in Section S5 example estimates of the apparent reaction velocity for varying target concentrations for five values of the time delay τ_{pre} ranging from 0 to 7 min.

Of course, at low target concentrations, τ_{MM} is much larger than τ_{pre}, and the late-readout effect is negligible. For instance, for $[E]_0$ = 1 pM, τ_{MM} > 20 days. In such cases, the measured reaction velocity over the first minutes (even hours) of the reaction is a very good approximation of the initial reaction velocity.

We can also define a characteristic target concentration $[E]_{0,late}$ for which the finite reaction time τ_{pre} prior to signal recording affects estimates of reaction kinetics:

$$[E]_{0,late} \approx \frac{K_M}{k_{cat}\tau_{pre}} \tag{24}$$

We approximate the value of K_M/k_{cat} as the value ultimately estimated from the kinetics experiments (e.g., at the final incubation temperature of interest). This limit makes exploring high target concentrations difficult. Eq 24 should be interpreted as an order-of-magnitude estimate that is nevertheless helpful in designing CRISPR experimental protocols.

Experimental Validation of the Kinetic Model. We now present an experimental validation of the model presented in eqs 6−19. Figure 3 shows progress curves, i.e., the typical measurement of cleaved reporter concentration as deduced using the calibration eq S5. Figure 3a shows the progress curves for *trans*-cleavage experiments in the presence of 1 nM target. As expected, the concentration of cleaved reporter increases with time and this increase varies with initial substrate concentration. In parallel to *trans*-cleavage experiments, we measured the increase in fluorescence of solutions containing the same concentrations of reporters as those reported in Figure 3a, but we omitted one (or several) critical component of the CRISPR reaction. Figures 3b−d show progress curves in the absence of either the dsDNA target, gRNA, or LbCas12a enzyme. Figure 3e shows progress curves corresponding to reporters incubated in buffer at 37 °C in the absence of the Cas enzyme, DNA target, and gRNA (i.e., only in reaction buffer). Strikingly, all cases resulted in a slow, yet measurable increase in cleaved reporter concentration with time and, as expected for a first-order reaction, the rate of increase depends on the initial reporter concentration $[S]_0$. Furthermore, this increase is similar in magnitude regardless of the presence of the Cas enzyme, dsDNA target, or gRNA. This suggests that the observed rise in fluorescence is mainly due to the nonenzymatic reporter degradation. We also note that the deviation from linearity in Figures 3b−e may originate from photobleaching after prolonged exposure, which is not captured by our simple model. Importantly, all cases shown in Figure 3b−e correspond to the case $[E]_0$ = 0, resulting in no predicted fluorescence signal increase in the naïve Michaelis−Menten framework. Note that signal-vs-time curves of CRISPR reporters in the absence of CRISPR enzymes are extremely rare and to our knowledge have never been discussed (see Section S8).

Figures 4a and b show initial reaction velocities corresponding to the progress curves shown in Figures 3b−e, as a function of initial reporter (a.k.a. substrate) concentrations. Figure 4a shows data in a linear−linear plot, while Figure 4b shows the same data in a log−log plot for the sake of clarity. Initial reaction velocities in the presence of 1 nM target dsDNA (red

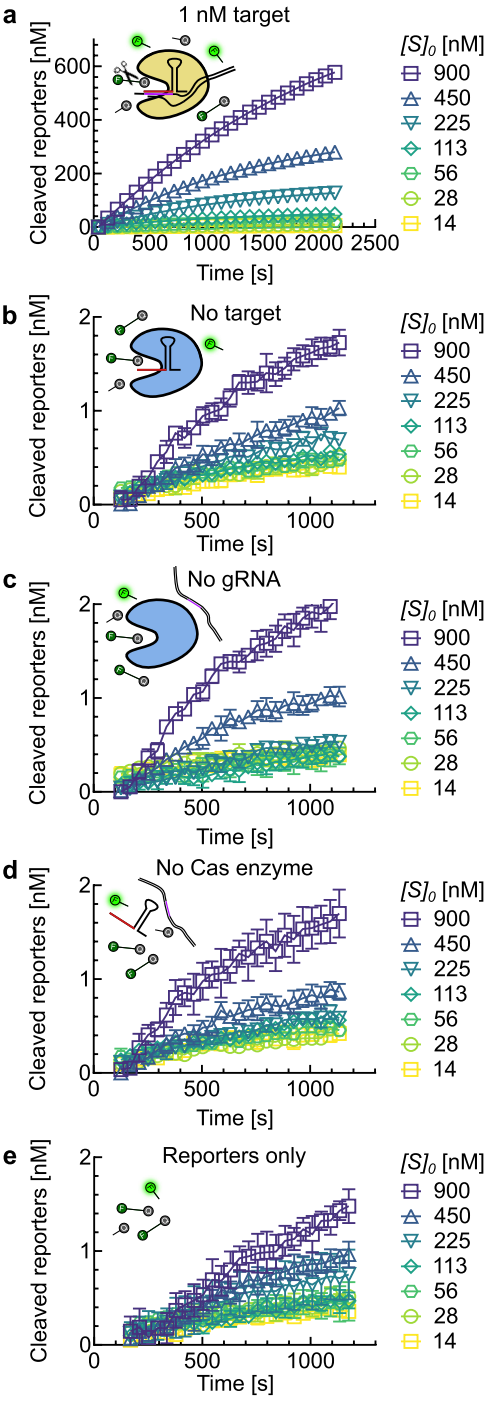


Figure 3. Measurements of the fluorescence signal from CRISPR assay reporters. (a) Progress curves with a target concentration of 1 nM (i.e., maximum value of $[E]_0$ = 1 nM) and eight representative values of the initial reporter concentration $[S]_0$. (b) Progress curves for the same chemistries as those in (a), but in the absence of target DNA. (c) Progress curves for the same chemistries as in (a), but in the absence of gRNA. (d) Progress curves for the same chemistries as in (a), but in the absence of Cas enzyme. (e) Progress curves for the same eight reporter concentrations as those in (a) in buffer only. The fluorescent signal is governed by reporter degradation at 37 °C. These experimental data were used to quantify reporter degradation rate constant k_{rep}.

https://doi.org/10.1021/acs.analchem.5c01060
Anal. Chem. XXXX, XXX, XXX−XXX

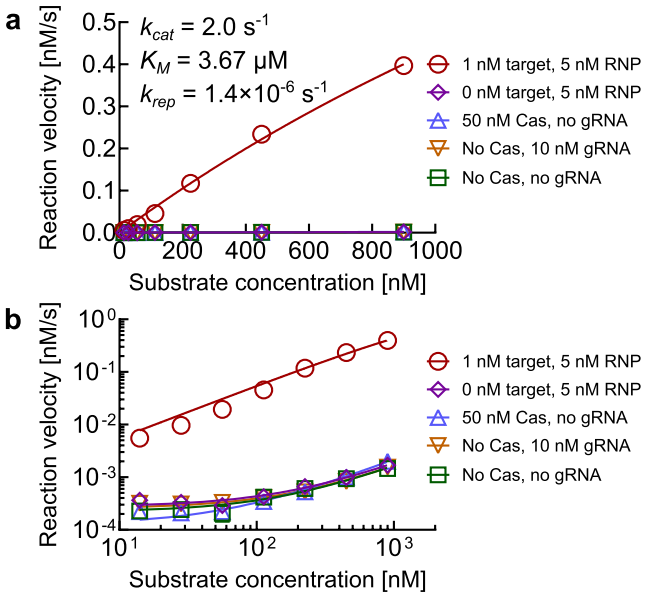


Figure 4. Initial reaction velocities vs substrate concentration for the different cases are presented in Figure 3. The experimental data in (a) is repeated in (b) with a logarithmic axis for clarity. Solid lines represent Michaelis–Menten fit (1 nM target case, red circles) or linear regressions (all other data).

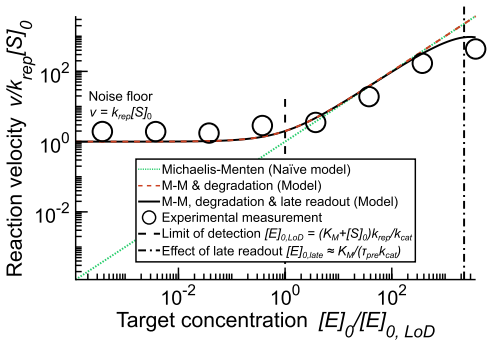


Figure 5. Measurements of maximum velocities of progress curves for LbCas12a activated by varied dsDNA target concentrations. The latter experimental measurements (circles) are compared to a prediction using the naïve Michaelis–Menten model (green dotted line, eq 5), the Michaelis–Menten model augmented with reporter degradation (orange dashed line, eq 16), and the augmented model with the effect of a "late readout," i.e., the effect of starting data acquisition delayed after the reaction starts (black solid line). At low target concentration, the apparent reaction velocity is governed by the reporter degradation rate $k_{rep}[S]_0$. Hence, reporter degradation imposes a limit of detection on CRISPR assays.

circles) were further fitted using the Michaelis–Menten model (eq 5) to extract values of k_{cat} and K_M for this specific gRNA sequence. The best fit for this data yields k_{cat} = 2.0 s^{-1} and K_M = 3.6 μM. These values are consistent with previously reported values for LbCas12a.[17,18] Also plotted in Figures 4a and b are the initial reaction velocities measured in the different cases reported in Figures 3b–e. Each data set was fitted using a linear regression (see eq 17). Regardless of the presence of the Cas enzyme, dsDNA target, or gRNA, the reaction velocity is well approximated by a single linear function of the initial reporter concentration. The collapse of the bottom four curves in Figure 4 constitutes further evidence that the background reaction velocity originates from the degradation of reporter molecules, which is not mediated by the Cas enzyme. A linear regression of the reaction velocities shown for reporters only (green squares) yields $k_{rep} = 1.4 \times 10^{-6}$ s^{-1}. To our knowledge, this measurement is the first quantification of the degradation rate of reporters in the absence of CRISPR enzyme. We also investigated the influence of temperature and fluorescence acquisition settings on this kinetic rate (see Sections S9 and S10), and found that the reporter degradation rate increases with both incubation temperature and the frequency of fluorescence readouts.

Experimental Validation of the Limit of Detection of CRISPR-Based Assays. Next, we experimentally investigated the effect of reporter degradation on the limit of detection of CRISPR-based assays. Figure 5 shows the measured reaction velocities for target concentrations ranging from 1 fM to 10 nM in our limit of detection experiments. To highlight the limiting effect of reporter degradation, reaction velocities were normalized using the product $k_{rep}[S]_0$, where $k_{rep} = 1.4 \times 10^{-6}$ s^{-1} (as measured earlier) and target concentrations were normalized using $[E]_{0,LoD}$, as estimated from eq 22 and the enzymatic rates measured above (k_{cat} = 2.0 s^{-1}, K_M = 3.6 μM). We also show in Figure 5 the corresponding predictions using three kinetic models: the naïve Michaelis–Menten model (green dashed line, eq 5), a simple version of our augmented model (orange dashed line, eq 16), and our augmented model further corrected for a late readout of the reaction velocity (black solid line). The latter model is computed using a numerical solution to the full augmented ODE system (eqs 8–15) wherein the reaction velocity is evaluated 5 min after the reaction has started (i.e., τ_{pre} = 5 min). The latter estimate is consistent with our experimental protocol.

Importantly, the reaction velocity measurements shown in Figure 5 exhibit the expected leveling off of signal as the target concentration decreases; a feature typical of sensitivity curves of many assays. As highlighted in the figure, the curve exhibits three regimes associated with low, intermediate, and high initial target concentrations. As a reference, we include in Figure 5 two vertical dashed lines to delineate these three regimes of the sensitivity curve.

The left-most vertical dashed line of Figure 5 highlights the value of $[E]_{0,LoD}$ as computed using the kinetic rates determined in the previous section. For target concentrations lower than $[E]_{0,LoD}$, the contribution of the reporter degradation to the signal is larger than that due to enzymatic *trans*-cleavage. In this regime, the reaction velocity becomes independent of the initial target concentration, effectively rendering the detection of the target impractical. In this regime, the measured saturation velocity is well approximated by the predicted noise floor reporter-cleaving rate of $k_{rep}[S]_0$ (again, using the measured value of $k_{rep} = 1.4 \times 10^{-6}$ s^{-1}). This behavior is well captured by both our augmented kinetics model (eq 16) and the numerical solution to the full ODE system, including late readout. This experimental saturation is, of course, not captured by the naïve Michaelis–Menten model, which predicts a proportional relationship between the target concentration and reaction velocity (see eq 5).

The second vertical line of Figure 5 highlights the value of $[E]_{0,late}$, as computed using the kinetic rates and τ_{pre} = 5 min. For target concentrations between $[E]_{0,LoD}$ and $[E]_{0,late}$, the *trans*-cleavage enzymatic activity dominates over reporter degradation and the target concentration is low enough that

https://doi.org/10.1021/acs.analchem.5c01060
Anal. Chem. XXXX, XXX, XXX–XXX

the late-readout effect is negligible. In this intermediate regime, all three models and experimental measurements agree.

For target concentrations larger than $[E]_{0,late}$, the late-readout effect becomes significant on the measurement of the reaction velocity. As detailed earlier, this typically results in an underprediction of the measured reaction velocity compared with the expected initial reaction velocity. As expected, only the augmented model corrected for the late-readout effect correctly captures the observed inflection in reaction velocity.

Finally, as additional experimental validation of our model, we compared our model to the experimental data published by Huyke et al.[17] The latter work reported sensitivity curves for three different Cas12 orthologs and 11 different gRNA sequences, and two different Cas13 orthologs. They performed Michaelis−Menten-type kinetics measurements for each of the 11 RNPs with both dsDNA and ssDNA targets for Cas12, and for four different Cas13 RNPs. Critical to the current comparison, their sensitivity measurements used a single fluorophore-quencher reporter type and a single reporter concentration ($[S]_0$ = 200 nM across all Cas12 sensitivity measurements, $[S]_0$ = 1 μM for Cas13 measurements). We provide in Section S11 the superposition of all sensitivity curves for Cas12 and Cas13. The fact that Huyke's sensitivity curves asymptote to approximately the same signal plateau at low target concentrations and across all Cas12 orthologs and 11 gRNA sequences, and across all Cas13 orthologs, is further strong evidence that the measured limits of detection are determined by reporter degradation and not by the kinetic rates of the various CRISPR enzymes.

Lastly, we note that DNA is usually very stable and typically not subject to cleavage in sterile solutions. However, there is strong evidence that dark quenchers are highly prone to degradation.[38−40] For example, Black Hole Quenchers (BHQ) and Iowa Black FQ quenchers contain azo functional groups, which may undergo reduction,[41] oxidation,[42] or photodegradation.[43,44] Hence, such degradation may result in the dynamic degradation of the reporter molecules which we observe.

CONCLUSION

We presented a new kinetic model for CRISPR *trans*-cleavage assays that use reporter molecules as a readout. The model captures the rise in fluorescence signal measured even in the absence of target molecules (and in the absence of CRISPR enzymes). We attributed this persistent rise in background signal to the kinetics of the degradation of the reporter molecules at 37 °C. Despite its immense importance and consequence in limiting the sensitivity of CRISPR assays, we know of no quantitative efforts to incorporate this effect into the interpretation of CRISPR assays. First, we modeled this degradation as a measurable, first-order decay. We also developed a novel kinetic model to account for the coupling between this degradation of reporters and the kinetics of *trans*-cleavage. The coupling of these reactions directly implies that the kinetics of cleaved reporters does not follow Michaelis−Menten kinetics. Second, we used our model to derive an analytical expression for a fundamental limit of detection of CRISPR assays that use fluorophore-quencher probes. Third, we validated our new model using experimental measurements of reporter cleavage rates. We also showed a comparison of our model with existing published data (in Section S11). The model shows excellent agreement with experimental data and shows that CRISPR assay limits of detection can be limited directly by reporter degradation.

The measurable rate of degradation of reporter molecules presents a fundamental limit to the sensitivity of any CRISPR-based assay that uses such probes. This has important consequences as the vast majority of published studies use fluorophore-quencher-type probes as the primary signal readout for CRISPR activity, including bulk assays but also droplet and microwell assays. It is likely that the reporter degradation rate depends on a variety of factors, including sequence, length, fluorophore type, and quencher type. Future work could also investigate degradation mechanisms of the reporter probes, including using specialized analysis techniques such as mass spectrometry. Moreover, assays that rely on the collateral activity of CRISPR-Cas enzymes but use different reporter compositions may also be subject to a similar background noise floor. This may include, for instance, lateral-flow assays that use biotin-labeled probes to distinguish positive from negative samples. The current results imply that the development of probes with repeatable and low degradation kinetic rates should be a major topic of research for studies aimed at increasing the sensitivity of CRISPR assays. Other possibilities for improvements include increasing the cleaved-to-uncleaved fluorescence ratio and increasing the catalytic efficiency of *trans*-cleavage.

ASSOCIATED CONTENT

Data Availability Statement

All the data presented in this study are available upon request to the authors.

Supporting Information

The Supporting Information is available free of charge at https://pubs.acs.org/doi/10.1021/acs.analchem.5c01060.

Signal Calibration: Basics and Improvements; Closed-Form Solution for the Michaelis−Menten System in the Low Target Limit; Analytical Solutions and Simulations Results for the Reaction Velocity; Estimation of the End point Fraction of Cleaved Reporters; Effect of Late Readout with Varying Delay Times; Influence of k_{rep} and k_{cat} on the Measured Reaction Velocity; List of Oligos Used in this Work; Calibration Protocol; Influence of Temperature on Reporter Degradation; Influence of Readout Frequency on Reporter Degradation; Comparison Between Current Augmented Model and 11 Sets of Published CRISPR-Cas12 Data and Four Sets of Published CRISPR-Cas13 Data; and Raw Fluorescence Signals (PDF)

AUTHOR INFORMATION

Corresponding Author

Juan G. Santiago − *Department of Mechanical Engineering, Stanford University, Stanford, California 94305, United States;* orcid.org/0000-0001-8652-5411; Email: juan.santiago@stanford.edu

Authors

Alexandre S. Avaro − *Department of Mechanical Engineering, Stanford University, Stanford, California 94305, United States; ESPCI Paris, Université PSL, CNRS CBI UMR 8231, Paris 75005, France;* orcid.org/0000-0003-1922-3629

Andrew D. Griffiths − *ESPCI Paris, Université PSL, CNRS CBI UMR 8231, Paris 75005, France*

https://doi.org/10.1021/acs.analchem.5c01060
Anal. Chem. XXXX, XXX, XXX−XXX

Complete contact information is available at:
https://pubs.acs.org/10.1021/acs.analchem.5c01060

Notes

The authors declare no competing financial interest.

REFERENCES

(1) Kaminski, M. M.; Abudayyeh, O. O.; Gootenberg, J. S.; Zhang, F.; Collins, J. J. *Nat. Biomed. Eng.* **2021**, *5*, 643−656.
(2) Kim, S.; Ji, S.; Koh, H. R. *Biomolecules* **2021**, *11*, 1162.
(3) Abudayyeh, O. O.; Gootenberg, J. S. *Science* **2021**, *372*, 914−915.
(4) Avaro, A. S.; Santiago, J. G. *Lab Chip.* **2023**, *23*, 938−963.
(5) Li, S.-Y.; Cheng, Q.-X.; Li, X.-Y.; Zhang, Z.-L.; Cao, S.; Gao, R.-B.; Zhao, G. P.; Wang, J.; Wang, J. *Cell Dis.* **2018**, *4* (1), 20.
(6) Chen, J. S.; Ma, E.; Harrington, L. B.; Da Costa, M.; Tian, X.; Palefsky, J. M.; Doudna, J. A. *Science* **2018**, *360*, 436−439.
(7) Gootenberg, J. S.; Abudayyeh, O. O.; Lee, J. W.; Essletzbichler, P.; Dy, A. J.; Joung, J.; Verdine, V.; Donghia, N.; Daringer, N. M.; Freije, C. A.; Myhrvold, C.; Bhattacharyya, R. P.; Livny, J.; Regev, A.; Koonin, E. V.; Hung, D. T.; Sabeti, P. C.; Collins, J. J.; Zhang, F. *Science* **2017**, *356*, 438−442.
(8) Li, S. Y.; Cheng, Q. X.; Liu, J. K.; Nie, X. Q.; Zhao, G. P.; Wang, J. *Cell Res.* **2018**, *28*, 491−493.
(9) Wang, S. Y.; Du, Y. C.; Wang, D. X.; Ma, J. Y.; Tang, A. N.; Kong, D. M. *Anal. Chim. Acta* **2021**, *1185*, 338882.
(10) Weng, Z.; You, Z.; Yang, J.; Mohammad, N.; Lin, M.; Wei, Q.; Gao, X.; Zhang, Y. *Angew. Chem. Int. Ed.* **2023**, *62* (17), No. e202214987.
(11) Zhang, J.; Lv, H.; Li, L.; Chen, M.; Gu, D.; Wang, J.; Xu, Y. *Front. Microbiol.* **2021**, *12*, 751408.
(12) Qian, S.; Chen, Y.; Xu, X.; Peng, C.; Wang, X.; Wu, H.; Liu, Y.; Zhong, X.; Xu, J.; Wu, J. *Anal. Biochem.* **2022**, *643*, 114593.
(13) Li, H.; Xie, Y.; Chen, F.; Bai, H.; Xiu, L.; Zhou, X.; Guo, X.; Hu, Q.; Yin, K. *Chem. Soc. Rev.* **2023**, *52*, 361−382.
(14) Azimzadeh, M.; Mousazadeh, M.; Jahangiri-Manesh, A.; Khashayar, P.; Khashayar, P. *Chemosensors* **2022**, *10*, 3.
(15) Chen, L.; Hu, M.; Zhou, X. *Trends Biotechnol.* **2025**, *43*, 98−110.
(16) Slaymaker, I. M.; Mesa, P.; Kellner, M. J.; Kannan, S.; Brignole, E.; Koob, J.; Feliciano, P. R.; Stella, S.; Abudayyeh, O. O.; Gootenberg, J. S.; Strecker, J.; Montoya, G.; Zhang, F. *Cell Rep.* **2019**, *26*, 3741−3751.
(17) Huyke, D. A.; Ramachandran, A.; Bashkirov, V. I.; Kotseroglou, E. K.; Kotseroglou, T.; Santiago, J. G. *Anal. Chem.* **2022**, *94*, 9826−9834.
(18) Ramachandran, A.; Santiago, J. G. *Anal. Chem.* **2021**, *93*, 7456−7464.
(19) Santiago, J. G. *QRB Dis.* **2022**, *3*, No. e9.
(20) Lv, H.; Wang, J.; Zhang, J.; Chen, Y.; Yin, L.; Jin, D.; Gu, D.; Zhao, H.; Xu, Y.; Wang, J. *Front. Microbiol.* **2021**, *12*, 766464.
(21) Yue, H.; Shu, B.; Tian, T.; Xiong, E.; Huang, M.; Zhu, D.; Sun, J.; Liu, Q.; Wang, S.; Li, Y.; Zhou, X. *Nano Lett.* **2021**, *21*, 4643−4653.
(22) Avaro, A. S.; Santiago, J. G. *Angew. Chem. Int. Ed.* **2022**, *61* (45), No. e202209527.
(23) Strohkendl, I.; Saifuddin, F. A.; Rybarski, J. R.; Finkelstein, I. J.; Russell, R. *Mol. Cell* **2018**, *71*, 816−824.
(24) Cofsky, J. C.; Karandur, D.; Huang, C. J.; Witte, I. P.; Kuriyan, J.; Doudna, J. A. *Elife* **2020**, *9*, No. e55143.
(25) Swarts, D. C.; Jinek, M. *Mol. Cell* **2019**, *73*, 589−600.
(26) Singh, D.; Mallon, J.; Poddar, A.; Wang, Y.; Tippana, R.; Yang, O.; Bailey, S.; Ha, T. *Proc. Natl. Acad. Sci. U. S. A* **2018**, *115*, 5444−5449.
(27) Gootenberg, J. S.; Abudayyeh, O. O.; Kellner, M. J.; Joung, J.; Collins, J. J.; Zhang, F. *Science* **2018**, *360*, 439−444.
(28) Feng, W.; Zhang, H.; Le, X. C. *Anal. Chem.* **2023**, *95*, 206−217.
(29) Shan, Y.; Zhou, X.; Huang, R.; Xing, D. *Anal. Chem.* **2019**, *91*, 5278−5285.
(30) Nalefski, E. A.; Sinan, S.; Cantera, J. L.; Kim, A. G.; Kooistra, R. M.; Rivera, R. E.; Janshen, J. P.; Bhadra, S.; Bishop, J. D.; Ellington, A. D.; Finklestein, I. J.; Madan, D. *Sci. Rep.* **2025**, *15* (1), 3909.
(31) Chen, J. S.; Ma, E.; Harrington, L. B.; Da Costa, M.; Tian, X.; Palefsky, J. M.; Doudna, J. A. *Science* **2021**, *360*, 436−439.
(32) Slaymaker, I. M.; Mesa, P.; Kellner, M. J.; Kannan, S.; Brignole, E.; Koob, J.; Feliciano, P. R.; Stella, S.; Abudayyeh, O. O.; Gootenberg, J. S.; Strecker, J.; Montoya, G.; Zhang, F. *Cell Rep.* **2021**, *34*, 108865.
(33) Blanluet, C.; Huyke, D. A.; Ramachandran, A.; Avaro, A. S.; Santiago, J. G. *Anal. Chem.* **2022**, *94*, 15117−15123.
(34) Schnell, S. *FEBS J.* **2014**, *281*, 464−472.
(35) Schnell, S.; Mendoza, C. *J. Theor. Biol.* **1997**, *187*, 207−212.
(36) Feng, W.; Peng, H.; Zhang, H.; Weinfeld, M.; Le, X. C. *Angew. Chem. Int. Ed.* **2024**, *63* (22), No. e202404069.
(37) Wu, X.; Li, J.; Nekka, F. *J. Pharmacokinet. Pharmacodyn.* **2015**, *42*, 151−161.
(38) Lesinski, J. M.; Khosla, N. K.; Paganini, C.; Verberckmoes, B.; Vermandere, H.; deMello, A. J.; Richards, D. A. *ACS Sens.* **2024**, *9*, 3616−3624.
(39) *I am having a problem with background drift with my BHQ™Probe. What might the cause be?*, LGC Biosearch Technologies. https://www.biosearchtech.com/support/faqs/qpcr-applications-calibration-troubleshooting/i-am-having-a-problem-with-background-drift-with-my-duallabeled-bhq-probe-what-might-the-cause-be.
(40) Ryabinin, V. A.; Kostina, E. V.; Sinyakov, A. N. *Nucleosides, Nucleotides Nucleic Acids* **2017**, *36*, 418−427.
(41) Kamenická, B. *J. Water Process. Eng.* **2024**, *61*, 105350.
(42) Oakes, J.; Gratton, P. *J. Chem. Soc., Perkin Trans.* **1998**, *2*, 1857−1864.
(43) Tanaka, K.; Padermpole, K.; Hisanaga, T. *Water Res.* **2000**, *34*, 327−333.
(44) Pozmogova, G. E.; Smirnov, I. *J. Biomol. Technol.* **2013**, *24*, S54.

https://doi.org/10.1021/acs.analchem.5c01060
Anal. Chem. XXXX, XXX, XXX−XXX